First-principles study of Fe and FeAl defects in SiGe alloys

A. Carvalho,[1,2] J. Coutinho,[3] R. Jones,[1] J. Goss,[4] M. Barroso,[3] and P. R. Briddon[4]
[1]*School of Physics, University of Exeter, Exeter EX4 4QL, United Kingdom*
[2]*Ceramics Laboratory, Swiss Federal Institute of Technology (EPFL), CH-1015 Lausanne, Switzerland*
[3]*I3N and Department of Physics, University of Aveiro, Campus Santiago, 3810-193 Aveiro, Portugal*
[4]*School of Natural Sciences, University of Newcastle upon Tyne, Newcastle upon Tyne, NE1 7RU, United Kingdom*
(Received 15 January 2008; revised manuscript received 7 July 2008; published 30 September 2008)

First-principles, spin-polarized local-density-functional calculations are used to model interstitial iron (Fe_i) and its complexes with substitutional aluminum in dilute Si_xGe_{1-x} alloys ($x<8\%$). We considered both the effect of direct bonding between Fe_i or Fe_iAl with Ge atoms in the $x\rightarrow 0$ limit and the evolution of the defect properties with the alloy composition. It is found that Fe_i prefers Si-rich regions, but when placed near a Ge atom, its (0/+) level is shifted toward the conduction band. However, the ionization energy of $Fe^{(+/+2)}$-Al^- is only slightly changed by the presence of neighboring Ge atoms in the proximity. It is also found that indirect alloying effects shift the donor levels of Fe_i and FeAl at a fast rate toward the valence band. The acceptor levels, however, remain approximately at the same distance from E_v.

DOI: 10.1103/PhysRevB.78.125208 PACS number(s): 61.72.Bb, 61.80.Az, 71.55.Cn

I. INTRODUCTION

Iron is one of the most unwanted contaminants in silicon-based integrated circuit technology. Often unintentionally incorporated during crystal growth or wafer processing, iron introduces deep levels in the gap, reduces the carrier concentration, and forms complexes and precipitates that degrade the device yield.[1] Although some understanding of iron contamination in silicon has been achieved,[1,2] the situation in SiGe alloys is far more complex. Additional degrees of freedom arise from the random Si and Ge atom distributions, modifying the basic defect properties, with consequent impact on the interaction with other point defects and on the efficiency of gettering techniques.[3,4] For example it was found that, as a consequence of the significant shift of the $Fe_i^{(0/+)}$ level with the Ge content, the concentration of iron driven to a high boron-doped region drops by one order of magnitude in $Si_{0.8}Ge_{0.2}$ relative to Si, reducing the gettering efficiency for Ge concentrations above 20%.[3] In order to understand the microscopic phenomena underlying this and other issues, theoretical information on the alloying effects and defect-Ge interaction is required.

The properties of interstitial iron (Fe_i) and its complexes have been the object of both experimental and theoretical studies, and an extensive review can be found in Ref. 2. Electron paramagnetic resonance (EPR) and electron-nuclear double resonance (ENDOR) found that Fe_i resides at the tetrahedral interstitial site (T) (Refs. 5 and 6) although Möessbauer spectroscopy reports suggest a lower symmetry configuration.[7] Two EPR centers have been associated with the defect. The spin-1 EPR signal associated with Fe_i^0 is replaced by a spin-3/2 signal of Fe_i^+ as the Fermi level crosses the donor level at about $E_v+0.40$ eV.[8] This is in line with Hall effect and resistivity measurements,[9,10] deep level transient spectroscopy (DLTS),[11–13] and optical methods,[10,14,15]which support the existence of a donor level between $E_v+0.36$ and $E_v+0.45$ eV.

In p-type silicon, ionized Fe_i is readily trapped by the acceptors. Complexes incorporating iron and B, Al, Ga, or In have been characterized by EPR, DLTS, Hall effect, and other techniques.[2] The formation of iron-acceptor pairs at temperatures below 80–100 °C is accompanied by a decrease in the concentration of isolated Fe_i, and they remain stable up to a higher temperature stage (100–200 °C) when a recovery of the concentration of isolated Fe_i is observed.[2]

The Fe_iB complex, formed by an interstitial iron close to a substitutional boron aligned along the ⟨111⟩ crystallographic direction,[16–18] has a well-known donor level at about $E_v+0.1$ eV. This electrical level arises from the $Fe_i^{+/+2}$ transition level, pulled into the band gap due to the electrostatic interaction with B^-.[17] Likewise, the $Fe_i^{0/+}$ level is shifted upward, giving rise to the $Fe^{0/+}B^-$ acceptor level at $\sim E_c-0.25$ eV. Donor levels of the trigonal centers Fe_iAl, Fe_iGa, and Fe_iIn, and the acceptor levels of Fe_iAl and Fe_iIn have also been detected or suggested.[2] Besides, an orthorhombic-I metastable structure has been observed for Fe_iAl,[19,20] Fe_iGa,[21] and Fe_iIn,[21,22] and tentatively identified for Fe_iB.[23]

Experimental evidence of the metastability of the Fe_iAl pair dates back to the DLTS work of Chantre and Bois in 1985.[24] It was shown that the pair can be reversibly cycled between the stable trigonal configuration, with a donor level at about $E_v+0.20$ eV, and the metastable orthorhombic structure with transition donor level at about $E_v+0.13$ eV. The metastable state can be populated by cooling down the p-Si sample under moderate reverse bias or light excitation.[19,24–27] Under such conditions, the iron atom becomes neutral, and thus only weakly bound to Al^-, and is easily promoted to the second-nearest-neighbor (NN) interstitial cage, forming the metastable center. Consequently, cooling the samples under illumination allows the EPR lines of the orthorhombic-I $\{Fe^+Al^-\}$ pairs to be observed, in addition to the trigonal spectra of nearest-neighbor $\{Fe^+Al^-\}$ and $\{Fe^{+2}Al^-\}$ pairs.[19,25]

Local-density-functional spin-polarized (LSDA) Green's function calculations[28–30] and recently fully relaxed generalized gradient approximation (GGA) calculations[18,31] were used to model the electronic structure of interstitial iron, reproducing the observed spin-1 and spin-3/2 for Fe_i and Fe_i^+,

respectively, and finding a donor level in the lower half of the band gap in agreement with experiment.

Iron-acceptor pairing was also the object of previous theoretical studies,[16–18] which found that the C_{3v} configuration is the most stable for Fe_iB but a C_{2v} configuration, where Fe_i is at the second-nearest T site of the substitutional acceptor atom, is almost degenerate in energy with the trigonal form for Fe_iAl and Fe_iGa, and energetically favorable for the larger acceptors In and Tl.[17,18] Both the orthorhombic and trigonal forms of each pair were found to exist in three charge states (−, 0, and +).[16–18] However, to our knowledge, modeling of either Fe_i or its complexes in SiGe has not been reported, perhaps due to the high computational effort involved in modeling random SiGe alloys.

Experimentally, Fe_i, Fe_iB, and Fe_iAl have been investigated in Si-rich SiGe alloys using EPR,[32] DLTS, and Laplace deep level transient spectroscopy (LDLTS).[4,13,26,27,33,34] Two types of alloying effects are apparent in the spectra. Firstly, with increasing Ge content the $Fe_i^{(0/+)}$ level is shifted toward the valence band much faster than it would be expected from the shrinkage of the band gap only, and the respective DLTS line becomes broader, reflecting the fluctuations in the local distribution of Ge.[13,32] Secondly, the LDLTS spectrum reveals the appearance of up to three satellite peaks around the dominant "no-germanium" main line.[34] The most prominent of those minor peaks is separated from the main band by about 40 meV,[26,27,34] and they are all related to short-distance Ge-Fe_i interactions.

If iron is paired with B or Al, the alloy pattern changes. In the case of the Fe_iAl defect, the alloy-induced shift and splitting of the donor level have been observed for the stable, ⟨111⟩-aligned pair as well as for the metastable ⟨100⟩-aligned pair in $Si_{1-x}Ge_x$ alloys with $x<3.2\%$.[26,27] Similarly to $Fe_i^{(0/+)}$, both Fe_iAl lines display a large alloy-induced shift of approximately $-1.0x$ eV toward the valence band although they arise from the $Fe_i^{(+/2+)}$ level.[26,34] For concentrations of about 3.2% of germanium, the donor level of the orthorhombic configuration becomes too close to the valence-band top to be detectable. The LDLTS spectra of each configuration show two satellite peaks on the higher energy side of the dominant no-germanium line. Curiously, the ratio between the integrated amplitudes of the main and subsidiary peaks is different for both configurations but independent on the cooling conditions. The separation between the subpeaks and the main line is only about 15 meV, smaller than the splitting observed for the Fe_i-Ge spectra.[26,27]

The present study aims to explore the rich behavior of the Fe_iAl complex in Si-rich SiGe alloys using density-functional theory calculations. We start by analyzing some practical issues related to the methodology, in particular to the treatment of the Fe atom (Sec. II). Sections III and IV are dedicated to the electronic structure of isolated interstitial iron in Si and SiGe. In Sec. V, we consider the Fe_iAl complex in silicon and relate our findings to previous calculations and to experiment. Then, Sec. VI considers the effect of a nearby Ge atom on the properties of this defect. Finally, we extend our study to dilute SiGe alloys in Sec. VII.

II. METHOD

We employed LSDA pseudopotential calculations, carried out using the AIMPRO code.[35] For the exchange and correlation energy (E_{xc}), a LSDA approximation was adopted unless otherwise stated.

The pseudopotentials used were generated by using the method of Hartwigsen, Goedecker, and Hutter (HGH),[36] where the $3s$ and $3p$ semicore orbitals of Fe were included explicitly among the valence electrons, and the $3d$ orbitals of Ge were treated by using a nonlinear core correction.[37] We note the importance of treating explicitly the $3s$ and $3p$ electrons of Fe, together with the $3d$ and $4s$ valence electrons. It has been previously shown that their interaction with the valence orbitals is essential to model Fe_iAl alloys.[38] Similarly, for the interstitial iron defect (Fe_i) in silicon, we found that, using the conventional $4s^23d^6$ valence configuration for iron, the spin states of the neutral and positive charge states (Fe_i^0 and Fe_i^+) are erroneously predicted to be 0 and 1 (0.7 and 1.1 eV lower in energy than the correct spin-1 and spin-3/2 states, respectively[39]). However, the correct spin states are obtained if the $3s$ and $3p$ orbitals of Fe are included explicitly among the valence electrons (more details will be given in Sec. III).

The valence orbitals are expanded in a set of (n_s,n_p,n_d) s-type, p-type, and d-type atom-centered Cartesian Gaussian basis functions, where (n_s,n_p,n_d) are (4,4,2) for Si, Ge, and Al, and (4,4,4) for Fe. Using this basis set, the lattice parameters and bulk modulus of Al (fcc) and ferromagnetic Fe (bcc) are predicted to be $a_0=3.98$ Å and $B=78.4$ GPa, and 2.75 Å and 278 GPa, respectively. These are to be compared with the experimental values $a_0=4.078$ Å and $B=75.5$ GPa for Al, and $a_0=2.861$ Å and $B=169.8$ GPa for Fe.[40] The overestimation of the bulk modulus of iron is a well-known shortcoming of LSDA.[41,42]

This raises a concern regarding the choice of the exchange-correlation functional. The contribution of the E_{xc} term to the total energy and magnetic effects was found to be crucial in modeling Fe (Refs. 41, 43, and 44) and FeAl alloys.[38,45] Calculations based on the LSDA for E_{xc} predict incorrectly that the energy per atom in nonmagnetic fcc Fe is about 0.08 eV lower than ferromagnetic bcc-Fe,[41] while a GGA calculation predicts the correct ordering.[43,44] On the other hand, both LSDA and GGA calculations predict stoichiometric $B2$-FeAl to be a ferromagnetic compound although it is known to be paramagnetic.[46–48] In the case of Fe_3Al, GGA predicts that the $L1_2$ structure has lower energy than the $D0_3$ phase, in conflict with experiment, while the LSDA gives the correct ordering.[49] A study of the exchange constant in Fe/c-FeAl/Fe systems obtained an overall qualitative agreement between LSDA and GGA calculations although with quantitative differences.[50]

Thus, although in the present paper we are mainly concerned with electric effects, we benchmarked the results obtained for the Fe_i and FeAl defects in silicon using the LSDA formulation of Perdew and Wang[51] against those obtained employing a GGA.[52] The calculations were performed using the Si lattice parameters optimized within LSDA and GGA, which are respectively $a_{Si}^{LSDA}=5.395$ Å and $a_{Si}^{GGA}=5.500$ Å [to be compared with the experimental value of 5.431 Å (Ref. 53)]. For interstitial iron, it was found that both LSDA and GGA calculations give the correct spin states ($S=3/2$ for Fe_i^+, and $S=1$ for Fe_i^0) although, as expected, the difference between high-spin and low-spin states is slightly larger when

the GGA is employed (see Sec. III).[39] Regarding the iron-acceptor pairs, the GGA does not seem to lead to a significant improvement over the LSDA results. In fact, as the binding between Fe_i^+ or Fe_i^{2+} and Al_s^- is predominantly electrostatic,[17,24] it is expected that the LSDA approximation, which in general holds more accurate bond lengths for semiconductors, and in particular for bulk Si and Ge,[54] will account better for the electrical properties of the defect. The sample calculations showed that, within the GGA, the orthorhombic configuration ($Fe_{T2}Al$) is erroneously predicted to be 0.09 and 0.06 eV lower in energy than the trigonal configuration ($Fe_{T1}Al$) in the neutral and positive charge states, respectively. The LSDA yields the same energy for the neutral structures but favors the trigonal structure by 0.06 eV in the positive charge state, in better agreement with experiment.[24] Indeed, the energy differences are very small, and become ~ 0.03 eV if the same lattice parameter is used (Sec. V). Hence, the local-density approximation will be employed to obtain the best estimates of the energies of the ground-state spin configurations.

The charge density and potential terms are expanded using a plane-wave basis set with a cut-off energy of 400 Ry. A convergence test for Fe_i showed that increasing this value to 800 Ry changed the total energy by only 0.03 meV. The Kohn-Sham levels are filled using second-order Methfessel-Paxton smearing[55] with a small, finite temperature chosen to improve the numerical stability of the self-consistency procedure.

Defects are placed in 64 atom cubic supercells, and the Brillouin zone (BZ) was sampled with the $MP-2^3$ special k-point sampling scheme of Monkhorst and Pack.[56] Sample calculations using $MP-4^3$ points showed that relative energies were converged with respect to BZ sampling.

Structural optimization of the atomic positions to minimize the total energy is performed using a conjugate gradient algorithm.[35] The accuracy required for the energy is 10^{-5} eV, and forces of less than 5×10^{-3} eV/Å are typically achieved.

Donor and acceptor levels were calculated using the semiempirical marker method (MM), which consists of comparing the electron affinities or ionization energies of the defects under scrutiny with the equivalent quantities calculated for well-known complexes (here referred as markers).[57] We take the electron affinity or ionization energy to be the absolute difference between the total energies of supercells containing the defect D in charge states q and $q+1$,

$$I(q,q+1) = \left|E(\mathrm{D}^q) - E(\mathrm{D}^{q+1})\right|. \quad (1)$$

A defect commonly used as marker is interstitial carbon (C_i). This defect assumes a $\langle 100\rangle$-split configuration in all the three charge states both in Si and in SiGe,[58,59] and in Si, it has well-known acceptor and donor levels at $E_c-0.10$ and $E_v+0.28$ eV.[60] Substitutional aluminum (Al_s) and interstitial iron were also used as markers, respectively, for the acceptor and donor levels of the Fe_iAl pairs.

Diffusion barriers are calculated using the climbing nudged elastic band (NEB) method.[61] All calculations start by setting initial and final structures, $\mathbf{Q}_0$ and $\mathbf{Q}_N$, respectively. The initial chain of intermediate structures $\mathbf{Q}_i$ with $i=1,\ldots,N-1$, named images, is generated by linear interpolation of the initial and final structures. We have used five images ($N=4$) in the calculations. Each pair of successive images is coupled by a virtual elastic band, and the atoms of each image are moved until the forces vanish. After three iterations of the regular NEB method, the highest energy image was allowed to move along the direction of the band (climb) to make sure that the saddle point was found.

The alloy was modeled by employing a series of $Si_{64-n}Ge_n$ supercells. The study was restricted to germanium concentrations below 8%, which corresponds to values of n between 0 and 5.

For each n, we generated 10 supercells by placing the germanium atoms in random positions of the silicon lattice. In previous work it was shown that the calculated lattice parameters reproduce well the structural properties of the alloys over all the concentration range[58] and that, for such small concentrations, Vegard's law is still a good approximation.[62] The lattice parameter for each Ge composition (a_x) can thus be estimated using the relation $a_x=(1-x)a_{\mathrm{Si}}+xa_{\mathrm{Ge}}$, where $x=n/64$, and $a_{\mathrm{Si}}=5.395$ and $a_{\mathrm{Ge}}=5.409$ Å are the calculated lattice parameters of Si and Ge. All the atomic positions were subsequently optimized using the conjugate gradient algorithm.

III. INTERSTITIAL IRON (Fe_i) IN Si

We modeled the electronic structure of interstitial iron in silicon by calculating the LSDA one-electron energy spectra of a $Si_{64}Fe_i$ supercell [Fig. 1(a)]. Here, we will assume that orbital angular momentum is quenched and spin-orbit coupling can be neglected.

The relative positions and occupancies of the levels are well described by the model of Ludwig and Woodbury. The $4s$ electrons of iron ($Fe:[Ar]3d^64s^2$) are transferred to the $3d$ shell, which is split into e and t_2 states by the tetrahedral crystal field. The e orbitals $d_{3z^2-r^2}$ and $d_{x^2-y^2}$ suffer greater repulsion from the second-nearest neighbors, and the respective energy level lies above t_2.

The electronic configuration for the neutral Fe_i defect is $t_2^6e^2$ with $S=1$ and 0.56 eV lower in energy than the spin-constrained $S=0$ state. The electrons in the partially occupied t_2 orbital are weakly bound, giving rise to a deep donor level. The $t_2^5e^2$ ($S=3/2$) state of the ionized defect ($^{3/2}Fe_i^+$) was found to be 0.24 eV lower in energy than the $t_2^6e^1$ ($S=1/2$) state, in agreement with previous calculations.[29,30] Employing a GGA for the exchange-correlation functional, the high-spin states are also favored, even by a higher energy difference: 0.83 eV for Fe_i^0 and 0.28 eV for Fe_i^+. This is also in line with a previous study.[18] We note that both the LSDA and the GGA approaches are known to favor high-spin states.[63]

The spin-3/2 configuration leaves the triplet partially occupied and sensitive to Jahn-Teller distortion. However, we found that iron remained stable at the T_d position upon perturbation in different directions.

Using C_i as marker, we estimate the position of the donor level of Fe_i to be $E_v+0.30$ eV, in good agreement with the experimental values that range from $E_v+0.36$ to $E_v+0.45$ eV.[2]

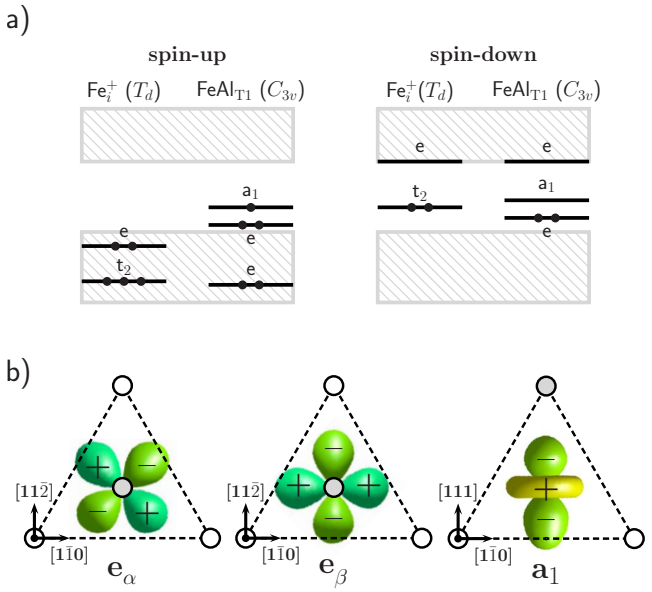

FIG. 1. (Color online) (a) Schematic of the positions of the calculated impurity-induced levels with respect to the bands of the host crystal. Levels are not to scale. (b) Representations of the wave function of the lower-lying doublet components (e_α and e_β) and a_1 one-electron states for the $Fe_{T1}Al$ defect. The e states, shown in the left-hand side, are projected on the (111) plane, whereas the a_1 state, shown in the right-hand side, is projected on the (11$\bar{2}$) plane. Si and Al atoms are represented by white and gray circles, respectively, and Fe, in the center of the tetrahedron, is hidden.

A. Formation energy

The formation energy at $T=0$ can be estimated as the energy required to bring an iron atom from a large $FeSi_2$ precipitate into the bulk of a silicon crystal,

$$E_f(\mathrm{Fe}_i) = E(\mathrm{Si}_{64}{:}\mathrm{Fe}_i) - E(\mathrm{Si}_{64}) - \mu_{\mathrm{Fe}}, \tag{2}$$

where μ_{Fe} is the chemical potential of an iron atom in $\gamma-FeSi_2$.[64] We obtain $E_f(\mathrm{Fe}_i)=2.21$ eV, about 0.9 eV lower than the formation energy of neutral Fe_s. Taking the number of available interstitial sites to be $N_i \sim 2\times 10^{22}$ cm^{-3} and ignoring entropy terms, we obtain a solubility $N_i \exp(-E_f/kT)$ of about 10^{13} cm^{-3} at 900 °C, within one order of magnitude of the experimental value calculated from the empirical expression $S_{\mathrm{exp}}=1.8\times 10^{28}\exp(-2.94/kT)$.[2]

IV. INTERACTION OF Fe_i WITH Ge ATOMS

A. Energetics

We then investigated the effect of a Ge atom in the close neighborhood of the Fe_i defect in the dilute alloy limit ($x\to 0$). For this purpose, we employed $Si_{63}Ge$ supercells constructed with the equilibrium constant of Si ($a_{\mathrm{Si}}=5.395$ Å). Selected Si atoms in a lattice position close to the interstitial Fe were substituted by Ge atoms and the total energies, obtained upon relaxation, were compared with that of a more distant Fe_i-Ge pair (about 8 Å apart), labeled Fe_i-Ge_{far}. Fe_i-Ge distances up to a fourth neighbor position were investigated. The respective pairs were labeled Fe_i-Ge_m, where m denotes the mth nearest-neighbor (mNN) lattice site relative to Fe_i. The presence of a Ge atom does not alter the preference for high-spin states.

TABLE I. Calculated formation energies change $[\Delta E(q)]$ for the Fe_i-$Ge_{m\mathrm{NN}}$ in the neutral, positive, and double positive charge states, relative to that of a Ge atom "far" from the defect. Level shifts $\delta I(0/+)$ and $\delta I(+/+2)$ with respect to the "far-germanium" level are also given. Positive δI values represent a shift toward the valence band. All energies are given in meV.

mNN	$\Delta E(2+)$	$\Delta E(+)$	$\Delta E(0)$	$\delta I(0/+)$	$\delta I(+/+2)$
1NN	127	126	166	−40	2
2NN	50	45	56	−11	5
3NN	0	−1	4	−5	1
4NN	7	4	10	−6	2
far	0	0	0	−0	0

In the three charge states of interest (+2 to 0), interstitial iron prefers to bond to Si rather than to Ge (Table I). The formation energy can be increased as much as 0.17 eV if one Ge atom bonds directly to Fe_i but even in a second-nearest-neighbor position its energy is increased by about 50 meV. This effect is amplified if more Si atoms in the neighboring shells are replaced by Ge. Thus, it is expected that Fe_i will avoid Ge-rich regions with a consequent decrease in the solubility and the mobility of the defect.

Accordingly, if the analysis is extended to SiGe, using as model the $Si_{64-n}Ge_n$ supercells generated as described in Sec. II, it is found that, despite the lattice expansion, the formation energy

$$E_f^n(\mathrm{Fe}_i) = E(\mathrm{Si}_{64-n}\mathrm{Ge}_n{:}\mathrm{Fe}_i) - E(\mathrm{Si}_{64-n}\mathrm{Ge}_n) - \mu_{\mathrm{Fe}}$$

invariably increases with n for any number of Ge atoms between one and five (for a given μ_{Fe}). However, the variance due to direct Fe_i-Ge interactions is quite large even if nearest-neighbor configurations are excluded. Hence, in order to quantify the net decrease in the solubility due to both direct and indirect interactions, it would be necessary to sample a much larger number of configurations than considered here, in a larger supercell, and account for the relative probability of each one of them, for example, in a Monte Carlo simulation.

B. Electrical levels

The effect of the presence of the Ge atom on the electrical level is only a small perturbation to the wave function and electrical levels of Fe_i. We can therefore calculate the small energy shifts of $Fe_i^{(0/+)}$ by subtracting the ionization energies of Fe_i-$Ge_{m\mathrm{NN}}$ to that of Fe_i-Ge_{far} (Table I). When a Ge atom is placed in the 1NN position, the distance of the donor level to the valence band is increased by about 40 meV, which is about the same separation of one of the closest DLTS subpeaks observed in previous work.[34] If two Ge atoms are placed at the NN sites (Fe_i-$2Ge_{\mathrm{NN}}$), the shift of the donor level is increased to 75 meV relative to Fe_i-$2Ge_{\mathrm{far}}$. This may be at the origin of a second subpeak, with a separation of

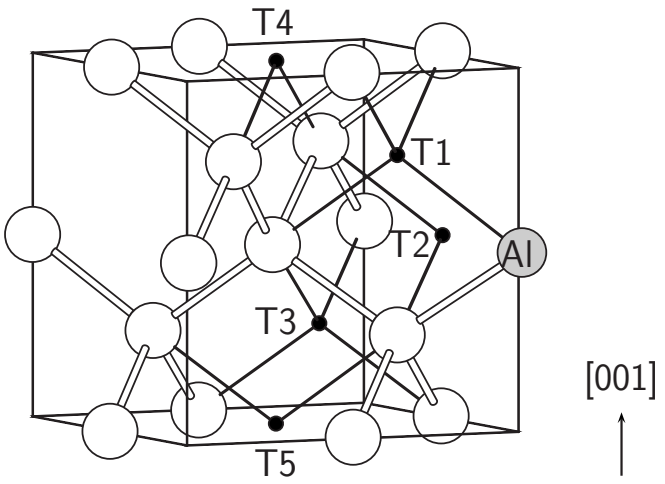

FIG. 2. Fe_iAl configurations proposed by Zhao *et al.* (Ref. 17) and considered in this paper. The Al and Si atoms are represented by gray and white spheres, respectively. Black points represent different possible positions of the Fe_i atom. *Tm* designates the *m*th neighbor interstitial *T* site.

about 80 meV, observed in the LDLTS spectra for higher concentrations.[34]

Alternatively, we could have chosen to compare the ionization energies of the Fe_i-Ge_{mNN} complexes with that of Fe_i in pure Si but the results would differ only by 0.6 meV from those presented in Table I. However, it seems that a major source of error may be the evaluation of the exchange-correlation functional. From a comparison between LSDA and GGA, we estimate the error to be about 15 meV. Hence, given this accuracy, we cannot confidentially do assignments of the subpeaks to specific atomic arrangements.

V. IRON-ALUMINUM COMPLEX IN Si

A. Electronic structure

We investigated several Fe_iAl configurations[17] formed by a Fe_i atom near an interstitial *T* site in the neighborhood of a substitutional Al atom. The Fe_iAl pairs, depicted in Fig. 2, are labeled as $Fe_{Tm}Al$ to designate the complex where Fe_i occupies the *m*th neighbor interstitial *T* site. The *T*1, *T*2, *T*3, *T*4, and *T*5 pairs are oriented along ⟨111⟩, ⟨100⟩, ⟨$3\bar{1}\bar{1}$⟩, ⟨111⟩, and ⟨111⟩ directions, respectively.

The presence of the Al atom results in a further splitting of the 3*d* states of iron (Fig. 1). Additionally, now one of the valence electrons of iron is transferred into the 3*p* shell of Al. The electronic configuration of Fe_iAl is obtained by placing the remaining 3*d* and 4*s* electrons of iron into the 3*d* states. We found that all the three charge states of the Fe_iAl complexes prefer a high-spin electronic configuration, in obedience to Hund's rule, although in some cases the energy difference between spin states is almost negligible (Table II).

Figure 1 illustrates the ground-state configuration of a [111]-aligned Fe^+Al^- ($Fe_{T1}Al$). The net valence of $\{Fe_iAl\}^q$ is the same as that in Fe_i^{q+1}, where $q=-1,0,1$. The degeneracy of the partially filled t_2 state of Fe_i is lifted in the presence of Al, and it hybridizes with the *e* state to form an a_1 and two *e* states of the C_{3v} point group [Fig. 1(a)]. The resulting gap states are an empty a_1 level and a filled *e* level, respectively, bonding and antibonding with respect to Al.

TABLE II. Calculated relative energies in the positive (E^+), neutral (E^0), and negative (E^-) charge states, with spin *S*; All energies are in electron volts.

		Model				
	S	T1	T2	T3	T4	T5
E^+	0	0.07	0.46	0.61	0.79	0.61
	1	0.00	0.06	0.38	0.45	0.22
E^0	1/2	0.11	0.33	0.45	0.54	0.36
	3/2	0.00	0.00	0.28	0.35	0.12
E^-	0	0.45	0.62	0.68	0.76	0.62
	1	0.00	0.11	0.17	0.21	0.08

$Fe_{T1}Al$ was found to be the lowest energy structure in the positive and negative charge states, whereas in the neutral charge state $Fe_{T1}Al$ and $Fe_{T2}Al$ yield approximately the same energy. Experimentally, both configurations have been observed, and it was shown that the trigonal structure $Fe_{T1}Al$ is 0.07 eV lower than the orthorhombic structure $Fe_{T2}Al$.[24] According to the calculations, the other trigonal configuration, Fe_iAl_{T5}, is also very low in energy (Table II).

From the experimental point of view, it is not clear whether neutral $Fe_{T1}Al$ and $Fe_{T2}Al$ defects have $S=1/2$ or $S=3/2$ since both descriptions account for the line splitting.[2,19,20,25]

In order to check the convergence of these results with the supercell size, we performed test calculations in 216 atom cells, employing the same BZ sampling and basis set. In that way, the $S=3/2$ spin state of the $Fe_{T1}Al$ structure was found to be 0.12 eV more stable than the $S=1/2$ state, and the $Fe_{T1}Al$ structure was found to be 0.08 eV higher in energy than the $Fe_{T2}Al$ structure. These results are in reasonable agreement with those obtained in supercells of 64 atoms (Table II) within the acceptable accuracy resulting from the approximations involved in the calculation.

1. Comparison between local-density-functional approximation and generalized gradient approximation

We also compared the results in Table II, obtained with LSDA, against a GGA calculation performed in identical conditions. The major difference is found in the energies of the unstable spin states: using GGA these tend to be about ~0.2 eV higher when comparing $S=1$ and $S=0$ states, and about ~0.1 eV higher when comparing $S=3/2$ and $S=1/2$ states.[63] This was to be expected, as both LSDA and GGA are known to favor the high-spin states. However, when comparing the ground-state electronic states, the magnitudes of the relative energies between different configurations of the FeAl defect are very close to those found using the LSDA. For example, the relative energies of the five neutral configurations investigated were found to be, from $Fe_{T1}Al$ to $Fe_{T5}Al$, respectively, 0.09, 0.00, 0.33, 0.41, and 0.17 eV, in agreement with the values presented in Table II. As pointed out in Sec. II, though, here also the LSDA seems to perform

TABLE III. Calculated $E(0/+)$ and $E(-/0)$ levels of $Fe_{T1}Al$ and $Fe_{T2}Al$ in silicon, obtained using the MM. The defects used as markers are given in brackets. All values are in electron volts.

level		defect			
		C_i	Fe_i	$Fe_{T1}Al$	$Fe_{T2}Al$
$E(0/+)-E_v$	MM(Fe_i)	0.38	Marker	0.29	0.24
$E(0/+)-E_v$	MM(C_i)	Marker	0.30	0.19	0.14
$E(0/+)-E_v$	Exp.	0.28[a]	0.40[b]	0.20[c]	0.13[c]
$E(-/0)-E_v$	MM(Al_s)	0.84		0.60	0.71
$E_c-E(-/0)$	MM(C_i)	Marker		0.34	0.23
$E_c-E(-/0)$	Exp.	0.10[a]			

[a]Reference 60.
[b]Reference 2.
[c]Reference 24.

better than the GGA. While with LSDA, the $Fe_{T1}Al$ and $Fe_{T2}Al$ structures are found to be degenerate in energy in the neutral charge state, and the $Fe_{T1}Al$ structure is more stable by 0.06 eV in the positive charge state; the GGA favors the $Fe_{T2}Al$ structure by 0.09 and 0.06 eV in the neutral and positive charge states, respectively. The discrepancy seems to arise mainly from the expansion of the lattice in the GGA calculation as these energy differences are reduced to 0.03 and −0.03 eV, respectively, if the LSDA lattice parameter is employed. Experimentally, the orthorhombic structure is found to be metastable in both charge states although by a small energy difference (0.07 in the neutral and 0.14 eV in the positive charge state).[24]

B. Electrical levels

The electrical levels were calculated using the marker method described previously.[57] The accuracy of the marker method is increased when the relevant states of the marker and of the defect under study have similar extent in space, and both lie close within the gap.[57] Here, different markers were used for comparison (Table III).

Using C_i as marker, it is possible to calculate both the donor and acceptor levels of the defects. The donor levels of $Fe_{T1}Al$ and $Fe_{T2}Al$ are placed at $E_v+0.19$ and $E_v+0.14$ eV, in excellent agreement with the experimental values of 0.20 and 0.13 eV, respectively. However, if Fe_i is used as marker (taking the experimental value of its $E(0/+)$ level to be $E_v+0.40$ eV), these values are raised by 0.1 eV.

The acceptor levels of $Fe_{T1}Al$ and $Fe_{T2}Al$, calculated using C_i as marker, are, respectively, $E_c-0.34$ and $E_c-0.23$ eV, again in good agreement with the results of a recent GGA calculation (giving $E_c-0.34$ and $E_c-0.21$ eV).[18] Using as marker Al_s, whose $(-/0)$ level lies at $E_v+0.057$ eV,[65] likely results in a systematic error, yielding $E(-/0)$ lower by about 0.2 eV than the levels obtained using C_i as marker. This is an expected consequence of the band-gap underestimation.

C. Transformation between $Fe_{T1}Al$ and $Fe_{T2}Al$

The transformation barriers between the two lowest energy structures, $Fe_{T1}Al$ and $Fe_{T2}Al$, were calculated using the NEB method described in Sec. II.

The activation energy required for the $Fe_{T1}Al \rightarrow Fe_{T2}Al$ reconfiguration is highly dependent on its charge state, decreasing with the net charge of the Fe ion: the calculated barriers are 0.82, 0.68, and 0.57 eV for $\{Fe_i^0Al^-\}$, $\{Fe_i^+Al^-\}$, and $\{Fe_i^{2+}Al^-\}$, respectively. These are in excellent agreement with the experimental values of 0.64 and 0.50 eV for $\{Fe_i^+Al^-\}$ and $\{Fe_i^{2+}Al^-\}$, respectively.[24] The equilibrium concentration ratio, however, depends only on the difference between their energies, $E(Fe_{T1}Al^q)-E(Fe_{T2}Al^q)$; it is thus expected that above ~100 °C the concentration of $Fe_{T2}Al$ defects originated by the $Fe_{T1}Al \rightarrow Fe_{T2}Al$ conversion is higher if the Fermi level lies above the donor levels of the defects.[24] A configuration-coordinate diagram for the two defects is presented in Fig. 3.

Having shown that the method used reproduces the energetic and electronic properties of the Fe_iAl complexes in Si in agreement with previous calculations and with experiment, we now generalize our study to the SiGe alloys.

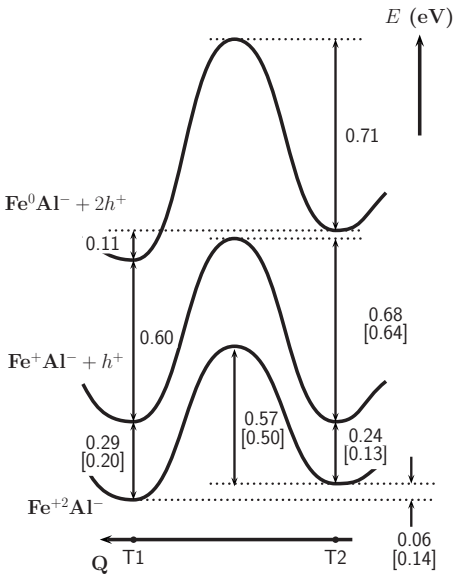

FIG. 3. Proposed configuration-coordinate diagram for the Fe_iAl defect in *p*-type Si. Experimental values from Ref. 24 are shown in square brackets. All the energies are given in electron volts.

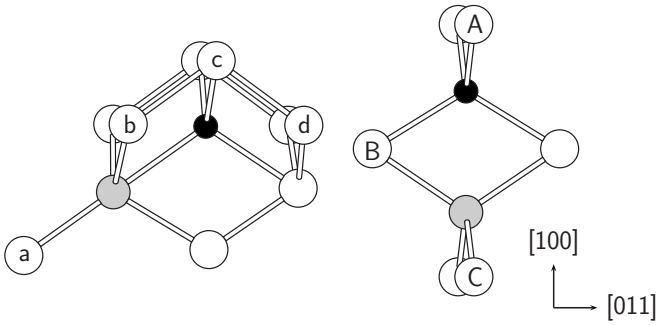

FIG. 4. Structures of $Fe_{T1}Al$ (left) and $Fe_{T2}Al$ (right) complexes in Si and SiGe. Si, Al, and Fe atoms are represented by white, gray, and black spheres, respectively. Si atoms labeled with letters were replaced by Ge atoms, forming $Fe_{T1}Al\text{-}Ge_{\alpha}$ and $Fe_{T2}Al\text{-}Ge_{\beta}$ complexes, with $\alpha=a$, b, c, or d, and $\beta=A$, B, or C.

VI. INTERACTION OF Fe_iAl WITH GE ATOMS

We have shown in Sec. III that Fe_i has a preference for Si-rich regions. In contrast, substitutional Al^- prefers to form Al-Ge bonds rather than Al-Si. The energy gain by placing one Ge atom bonding directly to Al is 60 meV. The lattice sites from the second-nearest neighbor onward are practically equivalent in energy.

To investigate whether Ge atoms stabilize the Fe_iAl complex, we computed the energies of the $Fe_{T1}Al$-Ge and $Fe_{T2}Al$-Ge complexes formed by replacing one of the Al or Fe_i first (silicon) neighbors by Ge atoms. The possibilities are depicted in Fig. 4. Their energies were compared to those of supercells containing $Fe_{T1}Al$ or $Fe_{T2}Al$ plus a remote Ge atom. The Fe_iAl-Ge complexes were optimized at the lattice parameter of silicon ($x\rightarrow 0$ limit).

In both cases, the complexes where Ge bonds directly to a Fe_i atom are energetically unfavorable (Table IV). These are $Fe_{T1}Al\text{-}Ge_c$ and $Fe_{T2}Al\text{-}Ge_A$, where "c" and "A" are the positions represented in Fig. 4. All the other Ge positions are almost equivalent in energy although there is a slight energy gain if a Ge atom bonds to the Al atom ($Fe_{T1}Al\text{-}Ge_a$ and $Fe_{T2}Al\text{-}Ge_C$).

The perturbed Fe_iAl levels are shifted toward the valence band. All shifts of the donor levels are very small and below the accuracy of the calculation ($\sim$15 meV). Experimentally, the DLTS subpeaks are observed in the higher energy side of the main Fe_iAl peaks but the shifts are also very small compared with the case of Fe_i.

VII. ALLOYING SHIFTS OF THE ELECTRICAL LEVELS

The presence of germanium atoms in the lattice modifies the properties of the host crystal, and consequently modifies the defect-matrix interaction as well. As a consequence, alloy-induced shifts and broadening of the DLTS and EPR lines associated with Fe are observed when the Ge concentration is increased.[13,32,34]

To model each defect D in a SiGe alloy with less than 8% of Ge content, we have generated a series of ten $Si_{64-n}Ge_n:D$ supercells with the n Ge atoms ($0\leq n\leq 5$) at random locations, as described in Sec. II. In order to isolate the long-range contribution, Ge atoms were not placed in the immediate neighborhood to the defects. All the other configurations were assumed to be equally probable. Since it was shown that from a second-nearest neighbor position onward the presence of the Ge atoms does not produce a significant splitting of the electrical level, this approximation does not affect the calculated shift of the level due to indirect effects.

The supercells were fully relaxed to compute $E(Si_{64-n}Ge_n:D)$ for each of the configurations, and the ionization energies or electron affinities of substitutional Al, Fe_i, $Fe_{T1}Al$, and $Fe_{T2}Al$ were averaged over all the configurations. The results are shown in Figs. 5 and 6, where the error bars represent the largest deviation from the average ionization energy/electron affinity, respectively. Although the number of configurations sampled was rather small, we can clearly notice the impact of alloy composition to the level drift. The relative deviations on the ionization energies/electron affinities also have an impact on the level broadening, but in order to quantify that effect, it would be necessary to sample a larger number of alloy configurations in larger supercells.

The alloy shifts can be computed using the marker method by comparing the ionization energies of defects in supercells with the same Ge concentration:[58]

$$E_D(q/q+1)|_x = E_M^{\text{exp.}}(q/q+1)|_x + I_D(q/q+1)|_x - I_M(q/q+1)|_x. \tag{3}$$

Thus, it is necessary to chose as marker a defect for which the level dependence with the germanium content [or for low

TABLE IV. Calculated changes in the formation energy [$\Delta E(q)$] for the $Fe_{T1}Al\text{-}Ge_{\alpha}$ and $Fe_{T2}Al\text{-}Ge_{\beta}$ complexes in the charge states $q=-1$, 0, and 1, relative to those of $Fe_{T1}Al$ and $Fe_{T2}Al$ with a remote Ge atom (far). Level locations $\delta I(0/+)$ with respect to the no-germanium level are also given. Positive $\delta I(0/+)$ values represent a shift toward the valence band. All energies are given in meV.

	$Fe_{T1}Al\text{-}Ge_{\alpha}$					$Fe_{T2}Al\text{-}Ge_{\beta}$			
α	$\Delta E(-)$	$\Delta E(0)$	$\Delta E(+)$	$\delta I(0/+)$	β	$\Delta E(-)$	$\Delta E(0)$	$\Delta E(+)$	$\delta I(0/+)$
a	−31	−37	−34	3	A	168	118	112	−7
b	11	−1	2	4	B	96	79	78	0
c	183	139	139	0	C	−56	−67	−72	−5
d	61	31	46	15					
far	0	0	0	0	far	0	0	0	0

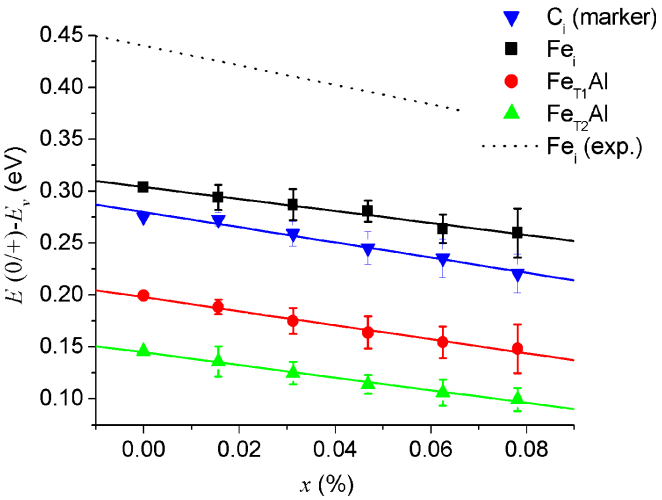

FIG. 5. (Color online) Donor levels of Fe_i and Fe_iAl complexes calculated using C_i as marker, as a function of the Ge concentration (x), along with the experimental level for Fe_i (Ref. 27).

concentrations the rate $\frac{dE}{dx}(q/q+1)]$ is known from experiment. This presents a difficulty since the experimental measurements of the level positions as a function of x in $Si_{1-x}Ge_x$ have been limited to a few defects and have large associated uncertainties.

Both the donor and acceptor levels of C_i have been found to shift away from the conduction band at a rate of approximately $0.30x$ eV in $Si_{1-x}Gex$ alloys with less than 50% of Ge content.[66] We thus use the C_i defect as marker for the donor levels. Its ionization energy, given by Eq. (1), is $I(0/+)=(5.463\pm0.002)-(1.09\pm0.05)x$ eV for $x<8\%$, and $E_M^{\text{exp.}}(0/+)=0.28-0.73x$, taking into account the $-0.43x$ eV narrowing of the band gap.[67]

Figure 5 shows the calculated donor levels of Fe_i, $Fe_{T1}Al$, and $Fe_{T2}Al$ for Si ($x=0$) and SiGe supercells with five com-

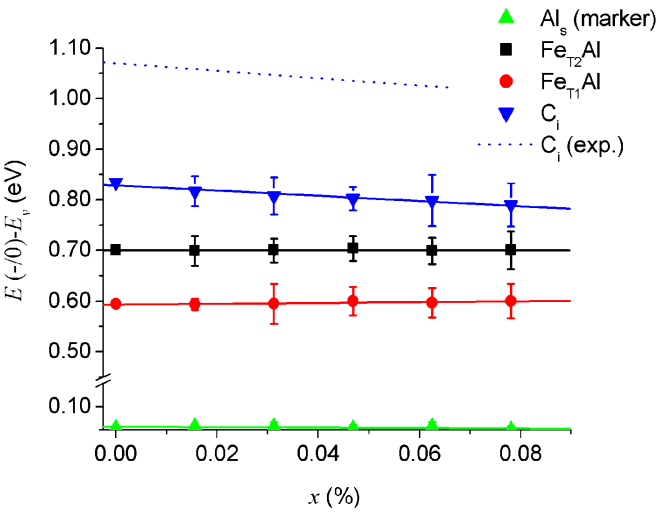

FIG. 6. (Color online) Acceptor levels of Fe_iAl complexes calculated using Al_s as marker, as a function of the Ge concentration (x). The calculated and experimental acceptor levels of C_i are also shown for comparison. The experimental values are taken from Ref. 66.

positions ($x=1/64$, 2/64, 3/64, 4/64, and 5/64), obtained using Eq. (3). The error bars represent the largest deviation from the average $E(0/+)$ value for each n. For the three defects, $E(0/+)$ shifts linearly with the germanium concentration in the interval considered, and approximately at the same rate $dE(0/+)/dx$, in agreement with experiment. The calculated slopes, obtained from a linear fit of the calculated points, are -0.58 ± 0.04, -0.67 ± 0.04, and -0.61 ± 0.03 eV, respectively. These are systematically underestimated as LDLTS measurements have found the respective values to be -0.94, -0.99, and -0.98 eV, respectively. However, they display the same ordering, indicating a slightly more rapid shift for the FeAl defects than for Fe_i.

A similar procedure can be used to find the variation in $dE(-/0)/dx$. Here we chose to use Al_s as marker rather than C_i since the calculated points have lower variance. Aluminum is a shallow acceptor following closely the dispersion of the valence band both in Si and in Ge. It is thus reasonable to assume that its ionization energy varies linearly between 0.057 eV for $x=0$,[65] and 0.0102 eV for $x=1$.[68] The calculated levels are shown in Fig. 6. We also evaluated the dependence of the position of the $C_i^{(-/0)}$ level for comparison, finding that it shifts toward the valence band at a rate of -0.51 ± 0.07 eV, in reasonable agreement with the $-0.73x$ eV dependence derived from experiment.[66] With regard to FeAl, we find that the levels of both $Fe_{T1}Al$ and $Fe_{T2}Al$ remain approximately at a constant distance from the valence band. The calculated $dE(-/0)/dx$ are 0.00 ± 0.03 and 0.08 ± 0.03 eV, respectively.

VIII. CONCLUSIONS

We considered both the effect of direct and indirect interactions of Fe_i and Fe_iAl with Ge atoms. It is found that Fe_i prefers Si-rich regions, and we suggest that this will contribute to an increase in the formation energy of Fe_i and a consequent decrease in the solubility with increasing germanium content.

If the iron atom is placed in the immediate neighborhood of a Ge atom, the shift of the $Fe_i^{(0/+)}$ level was estimated to be 40 ± 15 meV while the $Fe_i^{(+/+2)}$ ionization energy did not change within the accuracy of our calculation. The formation of a Ge-Fe bond rather than a Si-Fe bond costs approximately 0.1 eV. This is consistent with the suggestion that the Fe_i-Ge complex is responsible for one of the subpeaks observed in the LDLTS spectra of SiGe with less than 7% of germanium.[3]

Analogously, $Fe_{T1}Al$-Ge and $Fe_{T2}Al$-Ge complexes where iron bonds directly to Ge are energetically unfavorable, and the $Fe^{(+/+2)}Al^-$ levels are little changed by the presence of neighboring Ge atoms. The small shifts toward the valence band are predicted for some configurations but we have not found an assignment for the LDLTS subpeaks reported in the literature.[26,27]

Indirect alloying effects also have an impact on the electrical level of the defect. Using the marker method, it was found that the donor levels of Fe_i, $Fe_{T1}Al$, and $Fe_{T2}Al$ shift linearly toward the valence band with increasing Ge concentration ($x<8\%$) at a faster rate than the narrowing of the

band gap, consistent with experiment, a behavior which seems to be common to many impurity-induced donor levels in SiGe alloys.[27] In contrast, we found that the acceptor levels of $Fe_{T1}Al$ and $Fe_{T2}Al$ remain approximately at a constant distance from the valence band.

ACKNOWLEDGMENTS

The authors thank A. Mesli for his helpful comments. A.C. thanks *Fundação para a Ciência e Tecnologia* for financial support.

[1] A. A. Istratov, H. Hieslmair, and E. R. Weber, Appl. Phys. A: Mater. Sci. Process. **70**, 489 (2000).
[2] A. A. Istratov, H. Hieslmair, and E. R. Weber, Appl. Phys. A: Mater. Sci. Process. **69**, 13 (1999).
[3] A. Mesli, V. Kolkovsky, L. Dobaczewski, A. N. Larsen, and N. V. Abrosimov, Nucl. Instrum. Methods Phys. Res. B **253**, 154 (2006).
[4] K. Nauka and T. I. Kamins, Physica B **273-274**, 603 (1999).
[5] H. H. Woodbury and G. W. Ludwig, Phys. Rev. **117**, 102 (1960).
[6] S. Greulich-Weber, J. R. Niklas, E. R. Weber, and J. M. Spaeth, Phys. Rev. B **30**, 6292 (1984).
[7] P. Schwalbach, S. Laubach, M. Hartick, E. Kankeleit, B. Keck, M. Menningen, and R. Sielemann, Phys. Rev. Lett. **64**, 1274 (1990).
[8] H. Feichtinger, J. Waltl, and A. Gschwandtner, Solid State Commun. **27**, 867 (1978).
[9] C. B. Collins and R. O. Carlson, Phys. Rev. **108**, 1409 (1957).
[10] K. Wunstel, K. H. Froehner, and P. Wagner, Physica B & C **116**, 301 (1983).
[11] O. O. Awadelkarim and B. Monemar, J. Appl. Phys. **64**, 6306 (1988).
[12] H. Lemke, Phys. Status Solidi A **64**, 215 (1981).
[13] A. Mesli, B. Vileno, C. Eckert, A. Slaoui, C. Pedersen, A. N. Larsen, and N. V. Abrosimov, Phys. Rev. B **66**, 045206 (2002).
[14] H. Indusekhar and V. Kumar, Phys. Status Solidi A **95**, 269 (1986).
[15] S. Sakauchi, M. Suezawa, K. Sumino, and H. Nakashima, J. Appl. Phys. **80**, 6198 (1996).
[16] H. Overhof and H. Weihrich, Phys. Rev. B **55**, 10508 (1997).
[17] S. Zhao, L. V. C. Assali, and L. C. Kimerling, Mater. Sci. Forum **196-201**, 1333 (1995).
[18] M. Sanati, N. G. Szwacki, and S. K. Estreicher, Phys. Rev. B **76**, 125204 (2007).
[19] J. J. van Kooten, G. A. Weller, and C. A. J. Ammerlaan, Phys. Rev. B **30**, 4564 (1984).
[20] J.-M. Spaeth, S. Martini, and S. Greulich-Weber, Semicond. Sci. Technol. **13**, 725 (1998).
[21] W. Gehlhoff, P. Emanuelsson, P. Omling, and H. G. Grimmeiss, Phys. Rev. B **41**, 8560 (1990).
[22] W. Gehlhoff, P. Emanuelsson, P. Omling, and H. G. Grimmeiss, Phys. Rev. B **47**, 7025 (1993).
[23] H. Nakashima, T. Sadoh, and T. Tsurushima, Phys. Rev. B **49**, 16983 (1994).
[24] A. Chantre and D. Bois, Phys. Rev. B **31**, 7979 (1985).
[25] K. Irmscher, T. Kind, and W. Gehlhoff, Phys. Rev. B **49**, 7964 (1994).
[26] P. Kruszewski, A. Mesli, L. Dobaczewski, N. V. Abrosimov, V. P. Markevich, and A. R. Peaker, J. Mater. Sci.: Mater. Electron. **18**, 759 (2007).
[27] P. Kruszewski, Vl. Kolkovsky, A. Mesli, L. Dobaczewski, N. V. Abrosimov, V. P. Markevich, and A. R. Peaker, Phys. Rev. B **76**, 233203 (2007).
[28] A. Zunger, Phys. Rev. B **28**, 3628 (1983).
[29] H. Katayama-Yoshida and A. Zunger, Phys. Rev. Lett. **53**, 1256 (1984); Phys. Rev. B **31**, 7877 (1985); **31**, 8317 (1985).
[30] H. Weihrich and H. Overhof, Phys. Rev. B **54**, 4680 (1996).
[31] M. Sanati and S. K. Estreicher, Physica B **401-402**, 105 (2007).
[32] M. Hoehne, U. Juda, J. Wollweber, D. Schulz, J. Donecker, and A. Gerhardt, Mater. Sci. Forum **196-201**, 359 (1995).
[33] V. Kolkovsky, A. Mesli, L. Dobaczewski, N. V. Abrosimov, Z. R. Żytkiewicz, and A. R. Peaker, J. Phys.: Condens. Matter **17**, S2267 (2005).
[34] Vl. Kolkovsky, A. Mesli, L. Dobaczewski, N. V. Abrosimov, Z. R. Żytkiewicz, and A. R. Peaker, Phys. Rev. B **74**, 195204 (2006).
[35] P. R. Briddon and R. Jones, Phys. Status Solidi B **217**, 131 (2000).
[36] C. Hartwigsen, S. Goedecker, and J. Hutter, Phys. Rev. B **58**, 3641 (1998).
[37] S. G. Louie, S. Froyen, and M. L. Cohen, Phys. Rev. B **26**, 1738 (1982).
[38] C. D. Latham, S. Öberg, P. R. Briddon, and F. Louchet, J. Phys.: Condens. Matter **18**, 8859 (2006).
[39] The test system was a 64 atom Si supercell containing the Fe_i or Fe-Al defects, sampled with an $MP-2^3$ scheme.
[40] G. W. C. Kaye and T. H. Laby, *Tables of Physical and Chemical Constants*, 14th ed. (Longman, London, 1973); *American Institute of Physics Handbook* (McGraw-Hill, New York, 1957).
[41] C. S. Wang, B. M. Klein, and H. Krakauer, Phys. Rev. Lett. **54**, 1852 (1985).
[42] M. Körling and J. Häglund, Phys. Rev. B **45**, 13293 (1992).
[43] T. Asada and K. Terakura, Phys. Rev. B **46**, 13599 (1992).
[44] L. T. Kong and B. X. Liu, Appl. Phys. Lett. **84**, 3627 (2004).
[45] L. Vitos, P. A. Korzhavyia, and B. Johansson, Mater. Today **5**, 14 (2002).
[46] J. Zou and C. L. Fu, Phys. Rev. B **51**, 2115 (1995).
[47] J. Bogner, W. Steiner, M. Reissner, P. Mohn, P. Blaha, K. Schwarz, R. Krachler, H. Isper, and B. Sepiol, Phys. Rev. B **58**, 14922 (1998).
[48] N. I. Kulikov, A. V. Postnikov, G. Borstel, and J. Braun, Phys. Rev. B **59**, 6824 (1999).
[49] F. Lechermann, F. Welsch, C. Elsässer, C. Ederer, M. Fahnle, J. M. Sanchez, and B. Meyer, Phys. Rev. B **65**, 132104 (2002).
[50] J. M. Pruneda, R. Robles, S. Bouarab, J. Ferrer, and A. Vega, Phys. Rev. B **65**, 024440 (2001).
[51] J. P. Perdew and Y. Wang, Phys. Rev. B **45**, 13244 (1992).
[52] J. P. Perdew, K. Burke, and M. Ernzerhof, Phys. Rev. Lett. **77**, 3865 (1996).
[53] *CRC Handbook of Chemistry and Physics*, 81st ed., edited by D.

R. Lide (CRC, Boca Raton, 2000).
[54] J. Heyd, J. E. Peralta, G. E. Scuseria, and R. L. Martin, J. Chem. Phys. **123**, 174101 (2005).
[55] M. Methfessel and A. T. Paxton, Phys. Rev. B **40**, 3616 (1989).
[56] H. J. Monkhorst and J. D. Pack, Phys. Rev. B **13**, 5188 (1976).
[57] J. P. Goss, M. J. Shaw, and P. R. Briddon, Top. Appl. Phys. **104**, 69 (2007).
[58] A. Balsas, J. Coutinho, V. J. B. Torres, P. R. Briddon, and M. Barroso, Phys. Rev. B **70**, 085201 (2004).
[59] P. Venezuela, R. H. Miwa, and A. Fazzio, Phys. Rev. B **69**, 115209 (2004).
[60] L. W. Song, X. D. Zhan, B. W. Benson, and G. D. Watkins, Phys. Rev. B **42**, 5765 (1990).
[61] G. Henkelman and H. Jónsson, J. Chem. Phys. **113**, 9901 (2000); **113**, 9978 (2000).
[62] J. C. Aubry, T. Tyliszczak, A. P. Hitchcock, J.-M. Baribeau, and T. E. Jackman, Phys. Rev. B **59**, 12872 (1999).
[63] P. Mohn, C. Persson, P. Blaha, K. Schwarz, P. Novák, and H. Eschrig, Phys. Rev. Lett. **87**, 196401 (2001).
[64] K. A. Mäder, H. von Känel, and A. Baldereschi, Phys. Rev. B **48**, 4364 (1993).
[65] M. G. Holland and W. Paul, Phys. Rev. **128**, 30 (1962).
[66] A. Mesli and A. N. Larsen, J. Phys.: Condens. Matter **17**, S2171 (2005).
[67] J. Weber and M. I. Alonso, Phys. Rev. B **40**, 5683 (1989).
[68] T. H. Geballe and F. J. Morin, Phys. Rev. **95**, 1085 (1954).